Eur. J. Mech. B/Fluids, **18**, (1), 147-159, 1999

Numerical simulations of wake structure generated by rotating blades using a time marching, free vortex blob method

Duck Joo LEE *, Seon Uk NA

ABSTRACT. – Vorticity fields in the wake generated by rotating blades are calculated using a time-accurate, free vortex blob method without a non-physical model of the far wake. The computed free-wake geometry of a single rotor in hover is represented by three wake regions: a well-defined tip vortex region, an intermediate region, and an initially generated wake bundle. The simulated wake geometries in the radial and axial directions agree well with the experimental data for a two-bladed rotor for the overall regions of the wake. This agreement can be obtained by slowly increasing the rotational speed of the rotor blade, instead of using an impulsively rotating blade. The unsteady generation process of the wake structure is calculated for a single rotor with two blades. © Elsevier, Paris.

Nomenclature

$\vec{V}_{wake}(\vec{x},t)$	induced velocity due to the vorticity field in the wake.
$\vec{V}(\vec{x},t)$	blade surface velocity.
$\vec{n}(\vec{x},t)$	vector normal to the moving surface.
A_{ij}	normal-induced velocity coefficient on the i-th element of the blade due to the j-th element of the vortex lattice with unit circulation.
Γ_j	circulation value of the blade vortex lattice.
R_i	normal-induced velocity at each control point.
$\vec{\omega}_\sigma(\vec{x},t)$	vorticity field.
$\vec{\omega}^p(t)$	vorticity vector of the blob.
$\vec{\alpha}^p(t)$	strength vector (vorticity vector times volume) of the blob.
$\zeta_\sigma(\vec{r})$	smoothing function.
σ	smoothing radius.
vol^p	volume of the blob.
$k_\sigma(\vec{r})$	smoothed Biot-Savart Kernel.
$\vec{x}^p(t)$	vortex blob location.
$\vec{u}_\sigma(\vec{x}^p(t),t)$	local induced velocity of the vortex blob.

Superscripts

p, q	the vortex blob number.

1. Introduction

The flow field around a helicopter rotor is extremely complicated because of the wake generated by the rotating blades. Unlike fixed wings, flow around the rotors is intrinsically unsteady and the wake, especially the

* Correspondence and reprints.

Laboratory of Aeroacoustics, Department of Aerospace Engineering, Korea Advanced Institute of Science and Technology, 373-1, Kusong-Dong, Yusong-Ku, 305-701, Taejon, Korea.

0997-7546/99/01/© Elsevier, Paris

tip vortex, has an enormous influence on the flow field. Therefore, the helicopter wake geometry is critical in the estimation of helicopter performance and aerodynamic noise.

The hovering rotor wake can be represented by three wake regions: a well-defined contracted tip vortex region, an intermediate region, and an initially generated far wake bundle. The well-defined $3 \sim 4$ tip vortices have been properly correlated from experimental data for hovering flights (Landgrebe, 1972; Kocurek and Tangler, 1977) and reasonably predicted by numerous methods (Rosen and Grabe, 1988; Strawn and Barth, 1993; etc.). However neither correlation nor prediction has been attempted for the intermediate region because of lack of understanding of the phenomena. Even the correlation of the geometry of the first $3 \sim 4$ tip vortices is limited to blades of conservative shape. The tip geometries of highly twisted blades such as for the tilt rotor need to be modified based on new experimental data (Norman and Light, 1987). Therefore, the understanding and prediction of the rotor wake geometry are challenging problems in rotors.

Current methods of wake analysis for helicopter flow fields range from relatively simple momentum theory to lifting-surface methods with wake modelling (Baron and Boffadossi, 1993; Felker *et al.*, 1988; etc.). The difficulties of lifting-surface methods, in describing the stall and shock for the retreating and the advancing blade respectively, have led to recent efforts using computational fluid dynamics (CFD) codes, which are widely used in fixed-wing analyses (Srinivasan *et al.*, 1992; Strawn and Barth, 1993). Basically the CFD codes can describe the generation and transport of the vorticity in the wake. However, inherent numerical dissipation causes a rapid decay of the vortical structures. Serious problems occurring in the use of CFD codes are the far wake boundary conditions for hovering flight (Srinivasan *et al.*, 1992; Strawn and Barth, 1993), which is the same problem as for free-wake analyses.

To date, a prescribed wake (Landgrebe, 1972; Kocurek and Tangler, 1977), an iterative free-wake (Clark and Leiper, 1970; Rosen and Grabe, 1988; Felker *et al.*, 1988; Bagai and Leishman, 1995), and a time marching, free-wake model (Scully, 1975; Baron and Boffadossi, 1993) have been used successfully by many researchers to calculate the blade loadings in certain conditions. However, a more realistic wake geometry, which describes the overall regions of the wake has not been attempted or predicted using these methods. In addition, whether iterative or time marching free-wake methods, or CFD codes are used, the far-wake model and the artificial initial wake condition should be employed to obtain a converged steady solution in hover using the previous method. Typically, the far wake is modelled by a vortex ring (Clark and Leiper, 1970) or a semi-infinite cylinder (Rosen and Grabe, 1988), or the far wake is truncated after several spirals of the wake (Morino *et al.*, 1983). However, the initial wake state is critical, especially for the time marching method, because of the instability of the wake due to the strong starting vortex generated with the assumption of an impulsively starting blade, previously not taken into account. Therefore, a helicoidal spiral wake is used initially (Morino *et al.*, 1983) or a uniform axial velocity (Katz and Maskew, 1987) is superposed to allow for the impulsively starting condition. These methods make possible the movement of the initial vortex wake downward from the rotor disk to avoid problems of instability during the initial stage. However, a true transient solution and the wake evolutionary mechanism, which are critical in modelling ground effect or the fountain effect in tilt rotors during the hover condition cannot be predicted.

In this paper, a real time marching, free-wake method is described which does not need the non-physical initial condition and the far-wake model. The numerical problems occurring in wake systems are emphasized for the case of impulsively starting blades in order to understand the reasons for the instability in the wake system, whether it is physical, numerical or due to misuse of the initial condition.

These objectives can be fulfilled, not only by using an accurate numerical scheme, but also by observing the physical phenomena carefully. One of the key points is to show that the rotation speed must be increased slowly from zero to the required speed (Lee and Na, 1994), a factor that has been overlooked by many researchers. The unsteady wake mechanism is very important in predicting unsteady loading and noise, as well

as performance in conventional helicopter rotors, coaxial rotors or tilt rotors. Curved vortex filaments are used with the slowly starting blades (Lee and Na, 1994). The far wake is automatically formulated as the blades rotate. Therefore, the non-physical far wake model is not necessary. The calculations were carried out for 10 revolutions, which are enough for a converged solution of the air loads and the wake geometry. However, the intermediate region cannot be explained.

In the present work, the vortex segments are modeled as vortex blobs (Lee and Na, 1995), which are free to move independently according to the Biot-Savart law and the vorticity transport equation. Therefore, the stretching of the vorticity, occurring in three dimensions is calculated. The vortex blob method is especially useful for interaction problems occurring with coaxial rotors as well as wake-body interaction with typical rotors, because it might be easily applied when the lower rotor in the coaxial case interacts directly with the wake generated by the upper rotor. Whereas the vortex filament method, which describes the vortex region by connecting the point of each vortex element, is difficult to use to describe the direct interactions.

The mechanism of the intermediate unsteady region can be explained, which might be very important in predictions of unsteady loads and noise in certain flight conditions. The wake generated by a two-bladed single rotor is predicted and compared with experimental results. The unsteady generation process of the wake structure is calculated for thirty revolutions of the wake from a single rotor with two blades.

2. Formulation

The fluid surrounding the body is assumed to be inviscid, irrotational, and incompressible over the entire flow field, excluding the body's solid boundaries and its wakes. Therefore, a velocity potential $\Phi(\vec{x}, t)$ can be defined and the continuity equation in the inertial frame becomes:

$$\nabla^2 \Phi = 0. \tag{1}$$

The boundary condition requiring zero normal velocity across the body's solid boundaries is:

$$(\nabla \Phi + \vec{V}_{wake} - \vec{V}) \cdot \vec{n} = 0, \tag{2}$$

where $\vec{V}_{wake}(\vec{x}, t)$ is the induced velocity due to the vorticity field in the wake, $\vec{V}(\vec{x}, t)$ is the body surface's velocity, and $\vec{n}(\vec{x}, t)$ is the vector normal to the moving surface, as viewed from the inertial frame of reference. Since the governing equation does not depend directly on time, the time-dependency is introduced through the boundary condition (the location and orientation of the vector normal to the moving surface can vary with time).

Using Green's second identity, the general solution of Equation (1) can be constructed by integrating the contribution of the basic solution of source (σ) and doublet (μ) distributions over the body's surface:

$$\Phi(\vec{x}, t) = \frac{1}{4\pi} \int_{body} \mu \vec{n} \cdot \nabla \left(\frac{1}{r} \right) ds - \frac{1}{4\pi} \int_{body} \sigma \left(\frac{1}{r} \right) ds. \tag{3}$$

The resulting velocity induced by the combination of the source (σ) and doublet (μ) distributions is:

$$\nabla \Phi = \frac{1}{4\pi} \int_{body} \mu \nabla \left[\frac{\partial}{\partial n} \left(\frac{1}{r} \right) \right] ds - \frac{1}{4\pi} \int_{body} \sigma \nabla \left(\frac{1}{r} \right) ds. \tag{4}$$

Inserting Equation (4) into Equation (2) gives:

$$\left\{\frac{1}{4\pi}\int_{body}\mu\nabla\left[\frac{\partial}{\partial n}\left(\frac{1}{r}\right)\right]ds-\frac{1}{4\pi}\int_{body}\sigma\nabla\left(\frac{1}{r}\right)ds+\vec{V}_{wake}-\vec{V}\right\}\cdot\vec{n}=0. \tag{5}$$

The source term is neglected in the case of the blade airfoil. Thus, only the first part of Equation (4) is used to represent the lifting surface. The constant-strength doublet panel is equivalent to a closed vortex lattice with the same strength of circulation, ($\Gamma = \mu$). Then the induced velocity of the vortex lattice in Equation (5), representing the blade, can be formulated using the Biot-Savart law:

$$\vec{V}=-\frac{1}{4\pi}\int_{c}\frac{\vec{r}\times\Gamma d\vec{l}}{|\vec{r}|^3}. \tag{6}$$

The collocation point is at the mid-span and three-quarter chord of each lattice. The boundary condition of no-flow penetration is satisfied at the collocation point of each lattice. The application of the flow tangency condition (Eq. 5) to the vortex lattice distributions yields the following linear matrix equation that is to be solved:

$$A_{ij}\Gamma_j = R_i, \quad (i,j=1,\ldots,n), \tag{7}$$

where A_{ij} is the normal-induced velocity coefficient on the i-th element of the blade due to the j-th vortex lattice with unit circulation, and Γ_j is the unknown circulation value of the blade vortex lattice. R_i is the normal-induced velocity at each control point due to a free stream velocity, the blade-moving velocity, and the wake-induced velocity.

3. Time marching, free vortex blob method

A three dimensional wing trails the bound circulation (Γ) into the wake. Radial variation of bound circulation produces trailed vorticity in the wake, parallel to the local free stream direction at the instant it leaves the blade. Azimuthal variation of bound circulation produces shed vorticity, oriented radially in the wake. The strength of the trailed and shed vorticity is determined by the radial and azimuthal derivatives of bound circulation at the time the wake element leaves the blade. The bound circulation has a peak near the tip, and quickly drops to zero. The trailed sheet therefore has a high strength (proportional to the radial derivative of Γ) at the outer wake, and quickly rolls up into a concentrated tip vortex. The strength of the shed wake vortex at this time step is set equal to the one of the vortex lattice elements, which is located at the trailing edge of the blade ($\Gamma_{t.e.,t} = \Gamma_{wake,t}$). This condition is forced to satisfy the Kutta condition ($\gamma_{t.e.} = 0$).

The trailed and shed vortices in the rotor wake are modeled as vortex blobs, or in other words, as finite vortex sticks. A position vector and a strength vector are associated with each element. Each element can be thought of as a small section of a vortex tube. The element is convected by the local velocity and the strength vector is strained by the local velocity gradient. This method has the advantage that the blobs can move independently as they do not necessarily belong to a specific vortex filament for all times. This property is useful when calculating self-induced vortex interactions and interactions with other blades and the fuselage.

The blob representation of the vorticity field ($\vec{\omega}_\sigma$) is taken as

$$\begin{aligned}\vec{\omega}_\sigma(\vec{x},t) &= \sum_p \vec{\omega}^p(t)vol^p\zeta_\sigma(\vec{x}-\vec{x}^p(t)) \\ &= \sum_p \vec{\alpha}^p(t)\zeta_\sigma(\vec{x}-\vec{x}^p(t)),\end{aligned} \tag{8}$$

where $\vec{\alpha}^p(t)$ is a strength vector (vorticity vector times volume $= \vec{\omega}^p(t) vol^p$) of the blob. $(\vec{x} - \vec{x}^p(t))$ is the distance between the vortex blob at $\vec{x}^p(t)$ and the field point $\vec{x}$. The function $\zeta_\sigma(\vec{r}) = \frac{1}{\sigma^3}\zeta\left(\frac{|\vec{r}|}{\sigma}\right)$ is called the regulation or smoothing function, which is activated when the vortex blobs interact at close quarters. Without this function, a singular problem will occur. The symbol σ is a smoothing radius, and vol^p is the volume of the blob.

A 3D function is proposed by Winckelmans and Leonard (1993) giving a high order algebraic smoothing:

$$\zeta(\varepsilon) = \frac{15}{8\pi}\frac{1}{(\varepsilon^2+1)^{7/2}}, \quad \varepsilon = \frac{|\vec{r}|}{\sigma}. \tag{9}$$

Then the velocity field is obtained as

$$\vec{u}_\sigma(\vec{x},t) = \sum_p k_\sigma(\vec{x} - \vec{x}^p(t)) \times \vec{\alpha}^p(t), \tag{10}$$

where $k_\sigma(\vec{r}) = -\frac{1}{4\pi}\frac{\vec{r}}{|\vec{r}|^3}\zeta_\sigma(\vec{r})$ is the smoothed Biot-Savart Kernel.

The vortex locations $\vec{x}^p(t)$ move with the local velocity $\vec{u}_\sigma(\vec{x}^p(t),t)$. The vorticity vectors are also updated by the local strain field, in other words, the physical stretching of vorticity is calculated numerically, based on the vorticity transport equation:

$$\frac{\partial\vec{\omega}}{\partial t} + (\vec{u}\cdot\nabla)\vec{\omega} = (\vec{\omega}\cdot\nabla)\vec{u}. \tag{11}$$

The evolution equations for the vortex blob position and strength vector in the Lagrangian approach are taken as

$$\frac{d}{dt}\vec{x}^p(t) = \vec{u}_\sigma(\vec{x}^p(t),t), \tag{12}$$

$$\frac{d}{dt}\vec{\alpha}^p(t) = (\vec{\alpha}^p(t)\cdot\nabla^T)\vec{u}_\sigma(\vec{x}^p(t),t). \tag{13}$$

The equations obtained with the high order algebraic smoothing (9) are

$$\frac{d}{dt}\vec{x}^p(t) = -\frac{1}{4\pi}\sum_q \frac{(|\vec{x}^p - \vec{x}^q|^2 + \frac{5}{2}\sigma^2)}{(|\vec{x}^p - \vec{x}^q|^2+\sigma^2)^{5/2}}(\vec{x}^p - \vec{x}^q)\times\vec{\alpha}^q, \tag{14}$$

$$\begin{aligned}\frac{d}{dt}\vec{\alpha}^p(t) = \frac{1}{4\pi}\sum_q\Bigg[&\frac{(|\vec{x}^p - \vec{x}^q|^2 + \frac{5}{2}\sigma^2)}{(|\vec{x}^p - \vec{x}^q|^2+\sigma^2)^{5/2}}\vec{\alpha}^p\times\vec{\alpha}^q \\ &+ 3\frac{(|\vec{x}^p - \vec{x}^q|^2 + \frac{7}{2}\sigma^2)}{(|\vec{x}^p - \vec{x}^q|^2+\sigma^2)^{7/2}}(\vec{\alpha}^p\cdot((\vec{x}^p - \vec{x}^q)\times\vec{\alpha}^q))(\vec{x}^p - \vec{x}^q)\Bigg].\end{aligned} \tag{15}$$

Then the position $(\vec{x}^p(t))$ and the strength vector $(\vec{\alpha}^p(t))$ of the vortex blobs are simultaneously updated at each time step using the Biot-Savart law (14) and the vorticity transport equation (15). A second-order Runge-Kutta time integration is used to integrate Equation (14) and Equation (15).

A stable solution is obtained, because of the smoothing function in the core and the slowly starting rotor in the time marching, free-wake scheme.

The solution can be carried on until a converged solution for the well-defined tip vortex region near the rotor is found. It takes around $6 \sim 10$ revolutions. However, many more revolutions, roughly $20 \sim 30$, are required to compute the intermediate vortex region, the calculation of which was not attempted in the past.

4. Results and discussion

The wake geometry for a single rotor with one and two blades is calculated. For the one-bladed case, the aspect ratio of the blade is 6.54, the angular velocity of the rotor is 503 rpm (Rabbott, Jr., 1956) and the collective pitch angle is taken as 9.2 degrees. For the two-bladed case, the aspect ratio is 6.0, the tip Mach number is 0.439, and the collective pitch angle is taken as 8.0 degrees (Caradonna and Tung, 1981). The rotor blade is modelled using five chordwise panels and thirteen spanwise panels. Thirty time-steps are taken per blade revolution. The smoothing radius is 10% of the chord length. The same vortex modelling and smoothing parameters are used in calculating the wake geometry for both one and two-bladed rotors.

4.1. The impulsively and slowly starting rotor in hover

The impulsively starting rotor blade generates trailed and shed vortex wake elements. These wake elements are convected by the induced velocity of other wake elements and the self-induced velocity. Figure 1 shows the generation process of the rotor wake at each revolution for the impulsively starting case for the one-bladed rotor. The vortex elements generated near the root of the blade move upward initially and begin to move downward after several revolutions. Figure 2(a) shows tip vortex radial and axial locations for the one-bladed rotor. The instability of the impulsively starting wake is due to strong vortex shedding at the initial state. It can be explained as follows. The strength of the inner sheet is opposite in sign to the tip vortex. Therefore, the vortices located near the root tend to move upward due to the self-induced velocity and the induced velocity from the

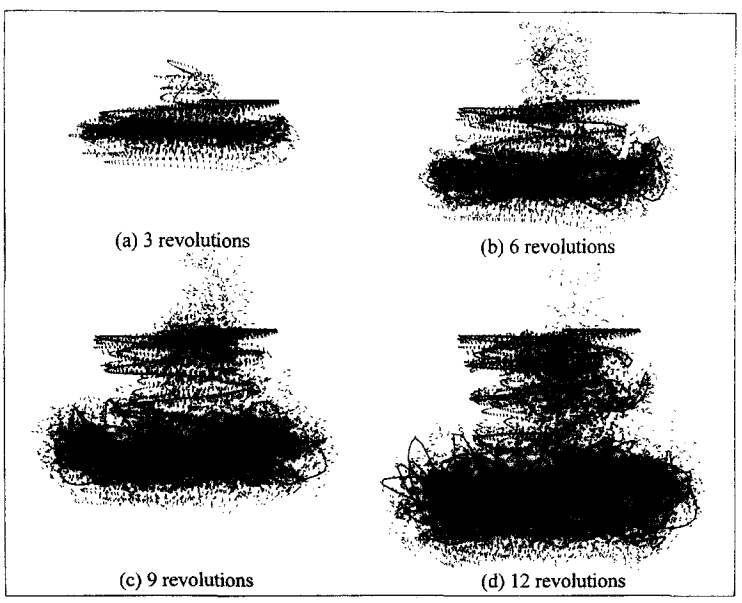

Fig. 1. – Wake generation process of the impulsively starting rotor with one blade.

other vortices in the inner sheet. The position of the root vortex is also influenced by the downward-induced velocity from the tip vortex. But, the influence of the inner vortex sheet is stronger than that of the tip vortex. Therefore the root vortex moves upward, as shown in Figure 1.

After several revolutions, the wake is developed, and the downward-induced velocity is sufficiently formed. Then, the root vortex moves downward and interacts with the inner vortex sheets and the tip vortex. But the location of the tip vortex is disturbed, due to the strong shed vortices at the initial state, as shown in Figure 2(a).

To remove the upward motion of the inner vortex sheet near the root at the initial state, several approaches have been attempted as mentioned in the introduction: enforcing a uniform downward flow initially (Katz and Maskew, 1987), using the far-wake model to suck the flow from the downward position through a vortex ring (Clark and Leiper, 1970), using a semi-infinite cylindrical vortex sheet (Rosen and Grabe, 1988), or starting from helical spirals of the wake (Morino *et al.*, 1983). These approaches are not, however, based on a real physical mechanism. A more realistic starting condition can be found in view of the real phenomena of helicopter rotors. That is, the rotor rotates smoothly from zero to a certain steady rotational speed. The rotor rotational velocity can be assumed to increase slowly from zero following the hyperbolic tangent function. The initial slope of

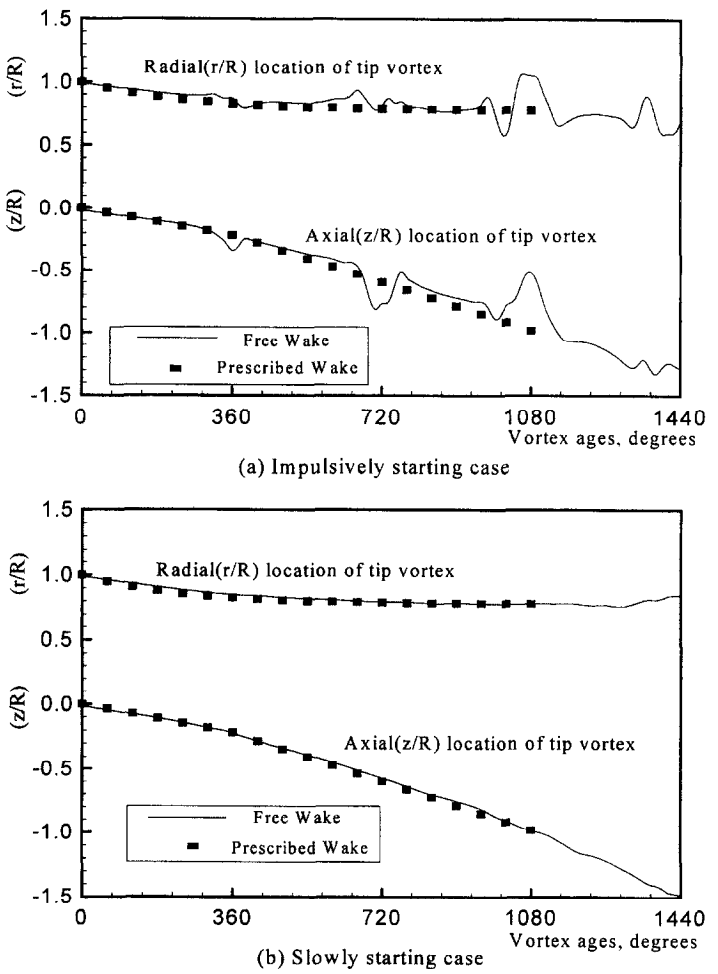

Fig. 2. – Tip vortex geometry of the impulsively and slowly starting cases for a one-bladed rotor.

this function is low. Then the strength of the initial wake is weak, the wake moves slowly downward, and the disturbance of the wake is suppressed.

Figure 2(b) shows that the radial and axial locations of the tip vortex for the slowly starting one-bladed rotor. The locations of the tip vortex are compared with the results obtained using the vortex lattice method for the blade with the wake geometry of Kocurek and Tangler (1977). The tip vortex wake geometry is not disturbed. Figure 3 shows the generation process of the rotor wake at each revolution for the slowly starting rotor with one blade.

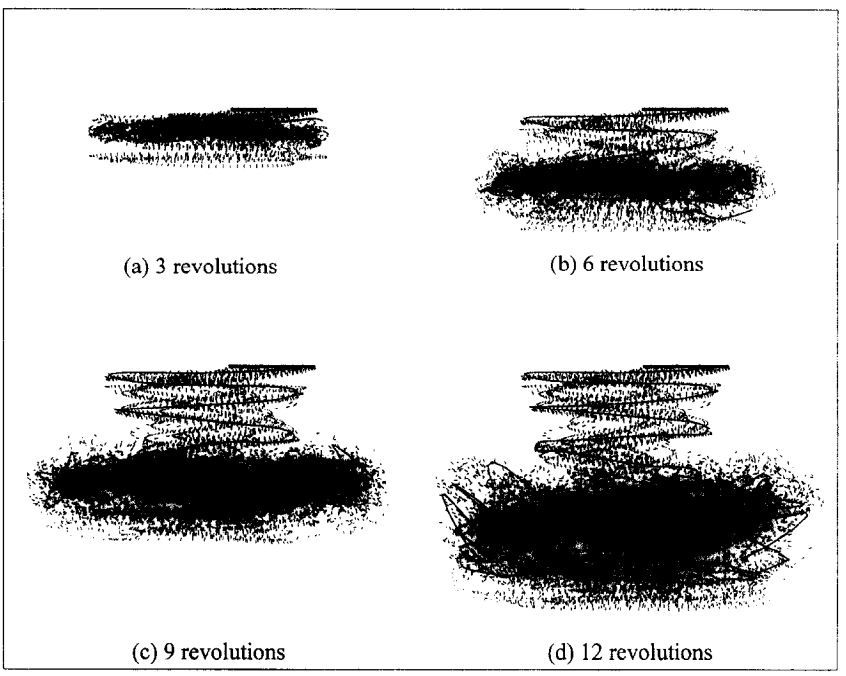

Fig. 3. – Wake generation process of a slowly starting rotor with one blade.

4.2. The wake structure of a rotor in hover with two blades

As the number of blades of the rotor increases, a larger number of wake elements are generated from the rotor blades at the same time. Then the induced velocity of wake elements is strong, and the steady flow field near the rotor is obtained with relatively few revolutions of the rotor blade.

The blades are started slowly to prevent the initial instability as shown in the case of one-bladed rotor.

The time history of the radial and axial locations of the tip vortex are shown in Figure 4(a). At least 10 revolutions of computations are necessary to have a converged tip vortex geometry up to approximately 540 degrees (one and a half revolutions) from the rotor blade. The time to obtain a converged solution near the rotor disk plane takes 2 hours on a SUN Enterprise 3000 server (167 Mhz cpu).

The radial and axial locations of the tip vortex at 10 revolutions are compared with the experimental results (Caradonna and Tung, 1981) as shown in Figure 4(b). The tip vortex contracts radially as the wake azimuthal angle increases. The axial descent rate of the tip vortex is constant up to 180 degrees for a two-bladed rotor (1st blade passage). After this azimuthal angle, the descent rate increases.

Figure 5 shows the generation procedure of the rotor wake at each revolution up to 12 revolutions for the slowly starting rotor with two blades. The inner wake sheet (generated from the blade trailing edge of the inner part of maximum bound spanwise circulation) and the tip vortex region interact and are convected downward.

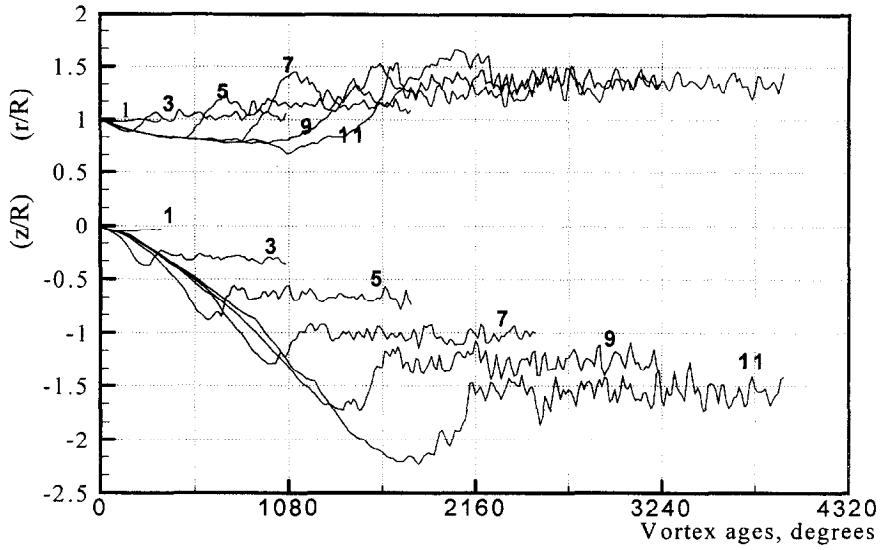

(a) Time history of the tip vortex position

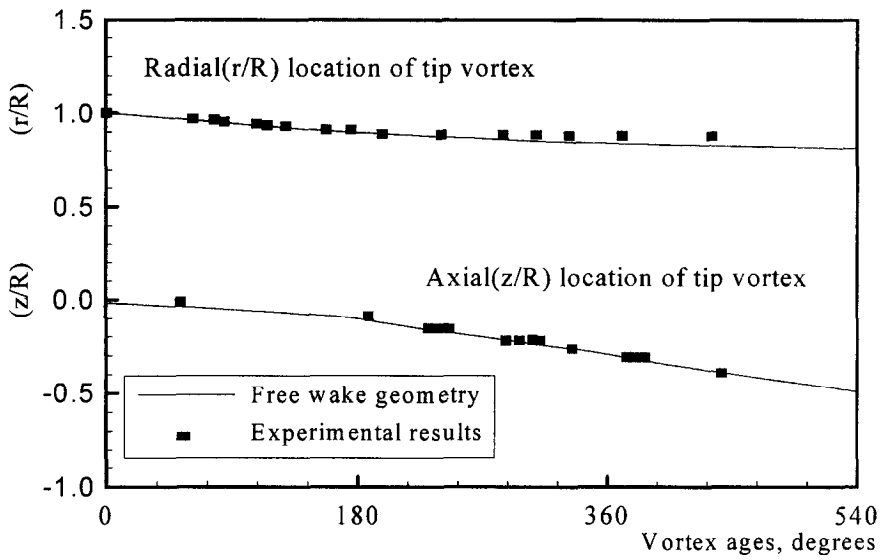

(b) Tip vortex geometry at 10 revolutions

Fig. 4. – Time history of the tip vortex axial and radial locations for a two-bladed rotor.

Figure 6 shows the side view of the tip vortex geometry generated from the two-bladed rotor at typical time steps near 20 revolutions. The tip vortex position is represented by connecting the points, which are the vortex centers of the trailed vortex blobs from the outer part of the maximum spanwise bound circulation. It is clearly seen that the tip vortices are rolled-up. The inner vortex sheets are calculated, but not plotted in the figure. During the initial stage, the wake elements which are generated by the rotor are expanded radially and easily disturbed because the flow field around the rotor is not yet formed enough to force the wake element to convect downward. This region is formed in the expanded wake bundle.

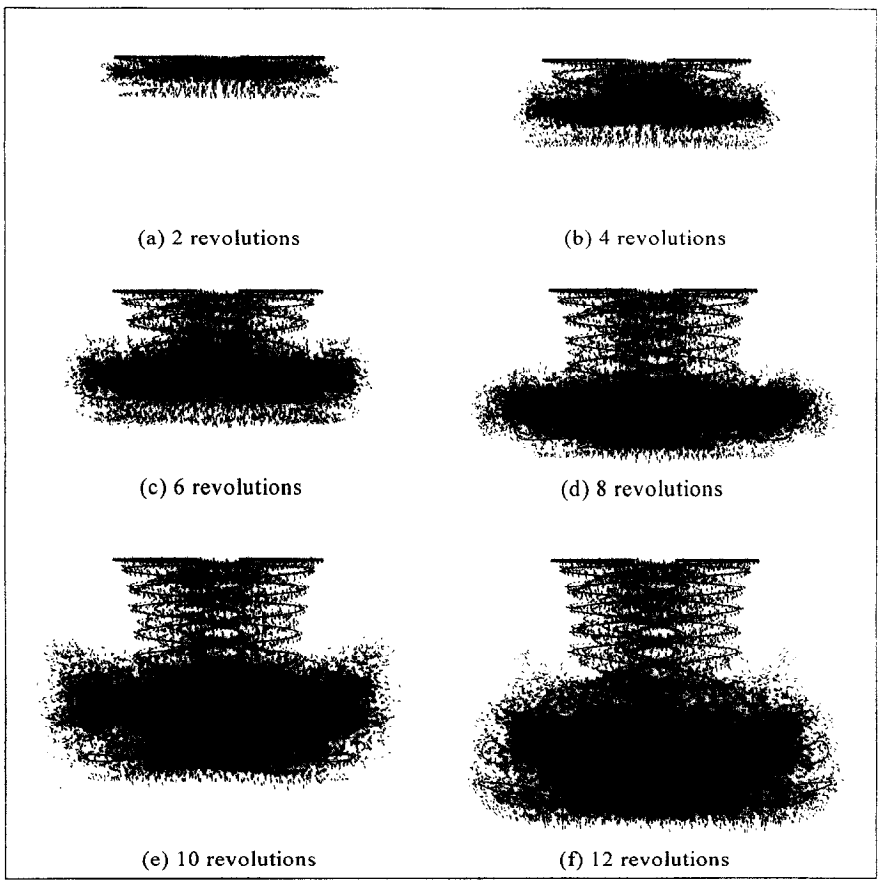

Fig. 5. – Wake generation process of the slowly starting rotor with two blades.

The tip vortices show a clear wake structure up to approximately 540 degrees (one and a half revolutions) from the blade trailing edge for the two-bladed rotor. Three or four tip vortices are clearly shown near the rotor disk plane in the sideview of the tip vortex geometry, as in the smoke visualization (Landgrebe, 1972).

Figure 7(a) shows that the cross-section of the calculated wake geometry near the rotor disk plane forms a well-defined wake structure of three or four tip vortices and an inner wake sheet.

When the region of the expanded wake bundle is moved downward and located far from the rotor, the induced effects of this region on the upper part of wake elements become small (after nearly 12 revolutions). The wake elements after maximum radial contraction start to be disturbed. Figure 6 also shows that the tip vortices, between the region of clear wake structure and the region of the expanded wake bundle, interact and are entangled with two or three revolutions of wake elements. This entangled tip vortex region moves downward into the wake bundle. The transition to the wake bundle is seen to occur through a leap-frogging motion of tip vortices, which motion is reported from recent experiments on the rotor wake (Caradonna *et al.*, 1997). The wandering phenomenon has been observed in experiments but could not be explained. Sometimes, it was claimed that this is because of the ground or experimental facility effect. However, based on the results for the wake in this paper, the wandering phenomenon is closely related to the leap-frogging motion of tip vortices. The smoke visualization indicates this region as shown in Figure 7(b).

Figure 8 shows the sideview of tip vortices near the rotor disk plane at various azimuthal angles. After the well-defined tip vortex region, the tip vortices begin to be disturbed and entangle with two or three revolutions

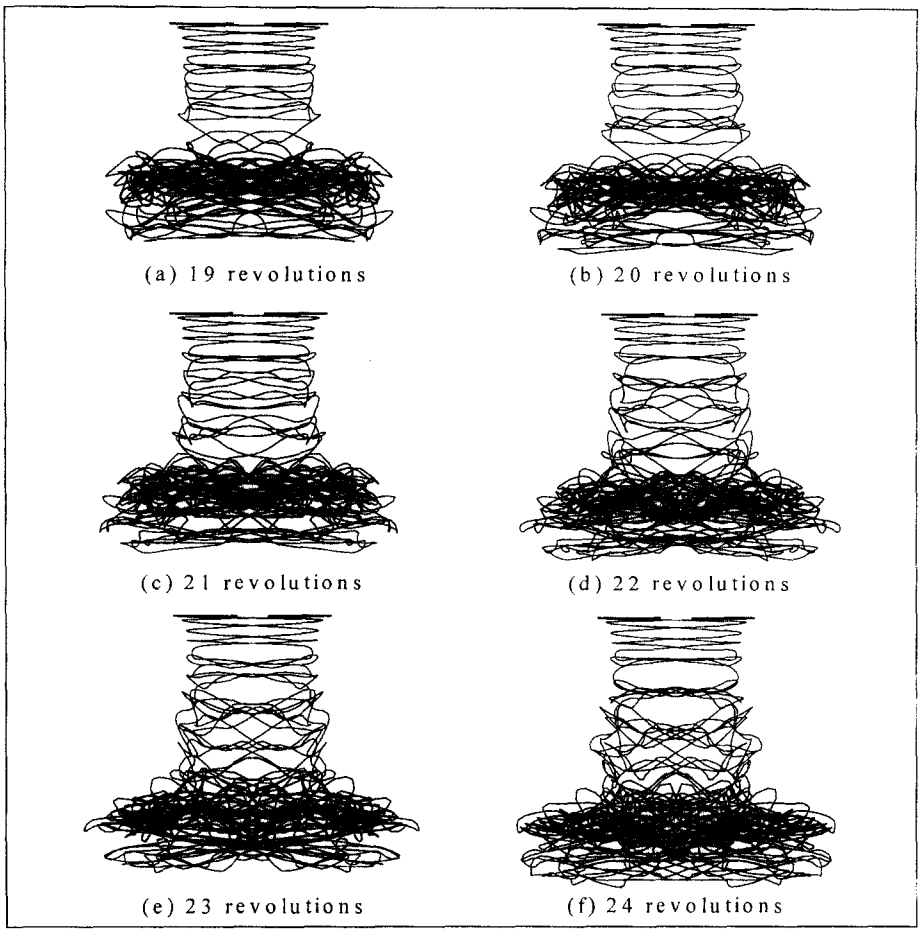

Fig. 6. – Evolution of the tip vortex geometry for a two-bladed rotor.

of the entangled wake elements. The well-defined tip vortex region near the rotor disk is not changed, but the tip vortices in the intermediate region are varied when viewed at different azimuthal angles.

The computed free-wake geometry of a single rotor in hover is represented by the three wake regions: a well-defined tip vortex region, an intermediate region, and an initially generated wake bundle.

5. Conclusions

Wake geometries of a single rotor in hover are calculated using a time-marching, free vortex blob method. The computed free-wake geometry is also (at least qualitatively) in agreement with the experimental wake mechanism which is represented by the three wake regions: a well-defined tip vortex region, an intermediate region, and the expanded wake bundle, which is generated at the initial stage.

The basic generation mechanisms of the rotor wake structure involving the far wake geometry are clearly understood from the time marching, free-wake calculations. The tip vortex region after a clear wake structure indicates that the vortex system is intrinsically unstable, and the classical wake concept, which is represented by a smoothly contracted tip vortex trajectory extending infinitely far down stream, is not realistic.

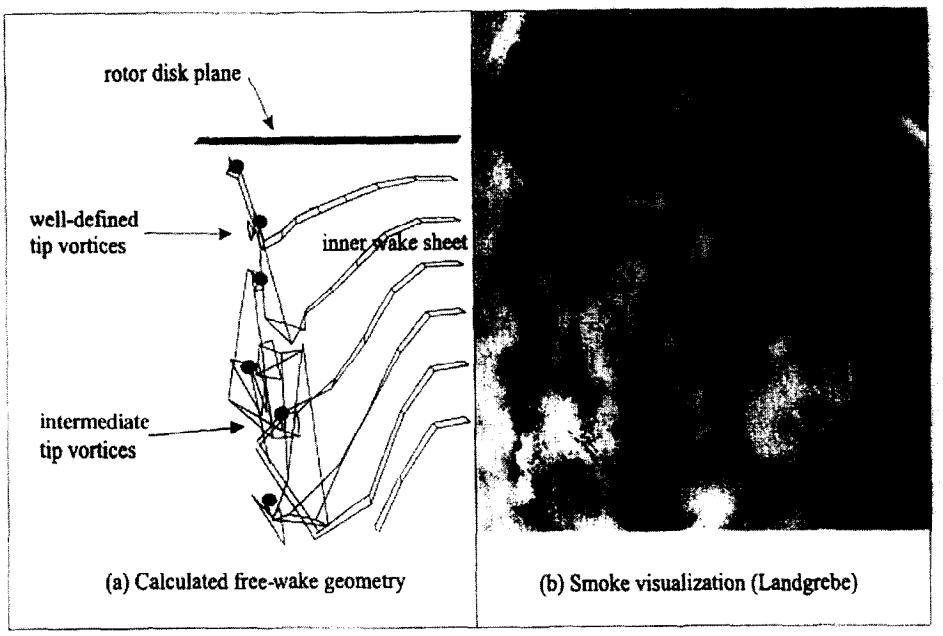

Fig. 7. – Cross-sections of the calculated free wake geometry near the disk plane for a two-bladed rotor.

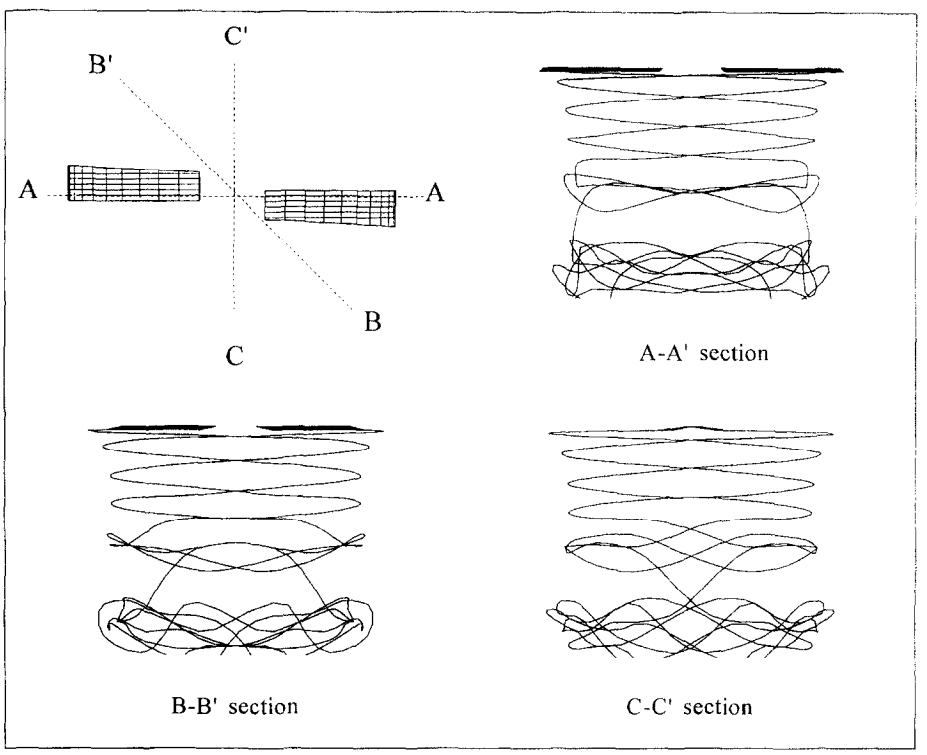

Fig. 8. – Sideview of the tip vortex geometry near the disk plane at various azimuth angles for a two-bladed rotor.

The wake geometries show excellent agreement with the experimental data in the two-bladed case. The radial and axial geometries of the tip vortex are calculated without a far-wake model. This can be done using a slowly starting rotor, based on the physical phenomena.

Therefore, a direct comparison between the computational results and experimental data is meaningless. However, the behavior of the entangled motion in the intermediate region is first shown in this paper. The smoke visualization of the region in the experiment can be partially explained. The measurements of the position in the intermediate region might be difficult because of the behavior of the unstable leap-frogging motion.

Not only is the well known contracted tip vortex shown as in the smoke visualization, but also the entangled tip vortices after clear tip vortices are well captured. The axial and radial position of the entangled tip vortices varies depending on the azimuthal angle in the intermediate region.

The definite wake geometry of the hovering rotor can only be obtained using a slowly starting rotor blade because the impulsively starting blade does not give a stable wake geometry.

REFERENCES

BAGAI A., LEISHMAN J. G., 1995, Rotor free-wake modeling using a relaxation technique - Including comparisons with experimental data, *J. Am. Helicopter Soc.*, **40**, 29–41.

BARON A., BOFFADOSSI M., 1993, Unsteady free wake analysis of closely interacting helicopter rotors, *Proc. 19th Eur. Rotorcraft Forum*, Cernobbio (Como), Italy, Sept. 14–16.

CARADONNA F. X., TUNG, 1981, Experimental and analytical studies of a model rotor in hover, *Vertica*, **5**, 149–161.

CARADONNA F., HENLEY E., SILVA M., HUANG S., 1997, An experimental study of a rotor in axial flight, *Proc. AHS Technical Specialists' Meeting for Rotorcraft Acoustics and Aerodynamics*, Williamsburg, VA.

CLARK D. R., LEIPER A. C., 1970, The free wake analysis a method for the prediction of helicopter rotor hovering performance, *J. Am. Helicopter Soc.*, **15**, 3–11.

FELKER F. F., QUACKENBUSH T. R., BLISS D. B., LIGHT J. L., 1988, Comparisons of predicted and measured rotor performance using a new free wake method, *Proc. 44th A. Nat. Forum, American Helicopter Society*, Washington, D.C.

KATZ J., MASKEW B., 1987, Unsteady low-speed aerodynamic model for complete aircraft configuration, *J. Aircraft*, **25**, 302–310.

KOCUREK J. D., TANGLER J. L., 1977, A prescribed wake lifting surface hover performance analysis, *J. Am. Helicopter Soc.*, **22**, 24–35.

LANDGREBE A. J., 1972, The wake geometry of a hovering helicopter rotor and its influence on rotor performance, *J. Am. Helicopter Soc.*, **17**, 3–15.

LEE D. J., NA S. U., 1994, Predictions of helicopter wake geometry and air loadings by using a time marching free wake method, *Proc. 1st Forum Russian Helicopter Soc.*, Moscow, Russia, 69–85.

LEE D. J., NA S. U., 1995, High resolution free vortex blob method for highly distorted vortex wake generated from a slowly starting rotor blade in hover, *Proc. 21th Eur. Rotorcraft Forum*, Paper No. II-5, Saint-Petersburg, Russia.

MORINO L., KAPRIELIAN Z., SIPCIC S. R., 1983, Free wake analysis of helicopter rotors, *Proc. 9th Eur. Rotorcraft Forum*, Stresa, Italy, Paper No. 3.

NORMAN T., LIGHT J., 1987, Rotor tip vortex geometry measurements using the wide-field shadowgraph technique, *J. Am. Helicopter Soc.*, **32**, 40–50.

RABBOTT J. P. Jr., 1956, Static-thrust measurements of the aerodynamic loading on a helicopter rotor blade, *NACA Technical Note 3688*.

ROSEN A., GRABE A., 1988, Free wake model of hovering rotors having straight or curved blades, *J. Am. Helicopter Soc.*, **33**, 11–19.

SCULLY M. P., 1975, Computation of helicopter rotor wake geometry and its influence on rotor harmonic airloads, *MIT ASRL TR 178-1*.

SRINIVASAN G. R., BAEDER J. D., OBAYASHI S., MCCROSKEY W. J., 1992, Flow-field of a lifting rotor in hover: A Navier-Stokes simulation, *AIAA J.*, **30**, 2371–2378.

STRAWN R. C., BARTH T. J., 1993, A finite-volume Euler solver for computing rotary-wing aerodynamics on unstructed meshes, *J. Am. Helicopter Soc.*, **38**, 61–67.

WINCKELMANS S., LEONARD A., 1993, Contributions to vortex particle metods for the computation of three-dimensional incompressible unsteady flows, *J. Comput. Phys.*, **109**, 247–273.

(Received 2 September 1996;
revised 5 November 1997;
accepted 7 April 1998.)